

Modeling Associative Plasticity between Synapses to Enhance Learning of Spiking Neural Networks

HaiBo Shen¹, Juyu Xiao¹, Yihao Luo¹ and Xiang Cao¹, Liangqi Zhang¹, Tianjiang Wang¹

¹Huazhong University of Science and Technology

{shenhaibo, juyuxiao, luoyihao, caoxiang112, zhangliangqi, tjwang}@hust.edu.cn

Abstract

Spiking Neural Networks (SNNs) are the third generation of artificial neural networks that enable energy-efficient implementation on neuromorphic hardware. However, the discrete transmission of spikes brings significant challenges to the robust and high-performance learning mechanism. Most existing works focus solely on learning between neurons but ignore the influence between synapses, resulting in a loss of robustness and accuracy. To address this problem, we propose a robust and effective learning mechanism by modeling the associative plasticity between synapses (APBS) observed from the physiological phenomenon of associative long-term potentiation (ALTP). In the proposed APBS method, synapses of the same neuron interact through a shared factor when concurrently stimulated by other neurons. In addition, we propose a spatiotemporal cropping and flipping (STCF) method to improve the generalization ability of our network. Extensive experiments demonstrate that our approaches achieve superior performance on static CIFAR-10 datasets and the state-of-the-art performance on neuromorphic MNIST-DVS, CIFAR10-DVS datasets by a lightweight convolution network. To our best knowledge, this is the first time to explore a learning method between synapses and an extended approach for neuromorphic data.

1 Introduction

Artificial neural networks (ANNs) have achieved the state-of-the-art performance in various tasks such as recognition and tracking [Lecun *et al.*, 2015]. However, there are some serious concerns about their huge demand of computational resources and power consumption [Li *et al.*, 2016]. Meanwhile, mammalian brains show it realistic to have superior cognitive abilities with extremely low power consumption [Akopyan *et al.*, 2015].

Inspired by the learning mechanisms of mammalian brains, spiking neural networks (SNNs) have been considered as a promising model for artificial intelligence (AI) and theoretical neuroscience [Roy *et al.*, 2019]. Unlike traditional neural

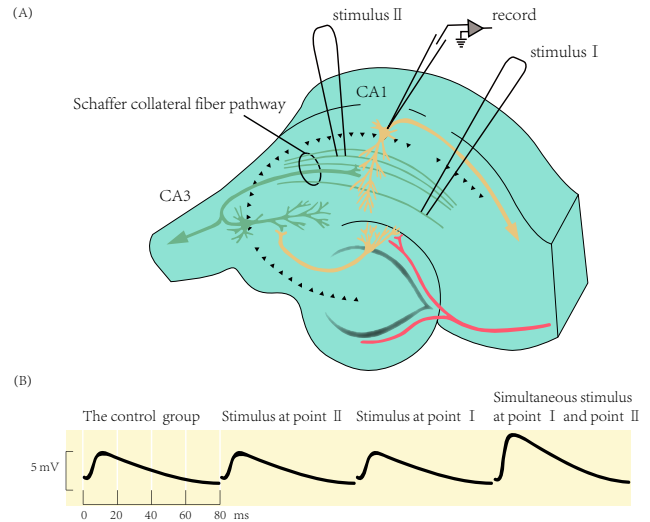


Figure 1: The associative long-term potentiation phenomenon in hippocampal slices of rats. (A) Two different groups of Schaffer collateral presynaptic fibers (stimulation I and stimulation II) are stimulated while performing intracellular recording of CA1 (cornu Ammonis) pyramidal cells. (B) The average response of CA1 pyramidal cells to a stimulus from point II is observed. The curve depicts the membrane voltage change after point I and point II are stimulated separately and simultaneously for ten minutes under control conditions. (referenced from [Barrionuevo and Brown, 1983].)

networks, SNNs transmit discrete spikes rather than real values between neurons. Therefore SNNs consume orders of magnitude less energy by enabling event-based computation, which can be carried out on neuromorphic chips [Akopyan *et al.*, 2015; Davies *et al.*, 2018]. Furthermore, SNNs are computationally more powerful than ANNs as the third generation of neural network models theoretically [Maass, 1997].

However, the non-differentiability of spike makes it unsuitable for traditional backpropagation, and the complete brain learning mechanism is far from clear, which poses significant challenges to the high-performance learning mechanism [Roy *et al.*, 2019].

Most successful learning methods of SNNs focus on learning between neurons, for example, brain-inspired biological methods [Zhang *et al.*, 2018], backpropagation methods with surrogate gradient [Wu *et al.*, 2021; Zheng *et al.*, 2021], and

other novel methods [Lagorce *et al.*, 2017; Sironi *et al.*, 2018; Cheng *et al.*, 2020]. When these methods only concentrate on learning between neurons and ignore the influence between synapses, some important information is also overlooked, making it difficult for efficient learning.

In this paper, we propose an Associative Plasticity Between Synapses (APBS) learning method inspired by the physiological phenomenon of associative long-term potentiation (ALTP). As shown in Figure 1 (A), point I and point II are stimulated, respectively, and the response of cells to point II is recorded for ten minutes. The results in Figure 1 (B) illustrate that the response is only enhanced when points I and II are stimulated simultaneously, indicating that there is a learning relationship between synapses. We model the associative plasticity between synapses by extracting shared weights, which is biologically plausible and computationally efficient. The shared weights build connections between synapses of the same neuron and transmit information when synapses are stimulated concurrently, which complements the learning mechanisms of SNNs. Since the biochemical mechanisms of this phenomenon may be different, we refine several update curves of the shared weights. Furthermore, we propose a spatiotemporal cropping and flipping (STCF) method for neuromorphic data augmentation, which enhances the temporal generalization ability of SNNs. Finally, we conduct extensive experiments to demonstrate the robustness and effectiveness of our methods.

Our key contributions are summarized as follows:

- We propose the APBS method inspired by the ALTP phenomenon, the first description of the interaction between synapses. By complementing the learning mechanism between synapses, APBS reduces information loss and improves accuracy.
- We propose the spatiotemporal cropping and flipping (STCF) method to enhance the temporal robustness of SNNs. To the best of our knowledge, it is the first data augmentation method suitable for neuromorphic data.
- We achieve superior performance on static CIFAR-10 datasets and the state-of-the-art performance on neuromorphic MNIST-DVS, CIFAR10-DVS datasets with a lightweight convolution network.

2 Related Work

2.1 Learning algorithm of SNNs

With the vigorous development of SNNs, various algorithms have been proposed to explore an efficient and robust SNNs learning algorithm, mainly divided into two categories.

The first is converted SNN, which converts some pre-trained non-spiking neural networks into SNNs with the same architecture. For example, [Ding *et al.*, 2021] proposes a rate norm layer to replace the ReLU activation function to get greater accuracy and better associate ANNs with SNNs. [Han *et al.*, 2020] proposes a "soft reset" spiking neuron model, referred to as residual membrane potential (RMP) spiking neuron, which retains the "residual" membrane potential above the threshold at the firing instants.

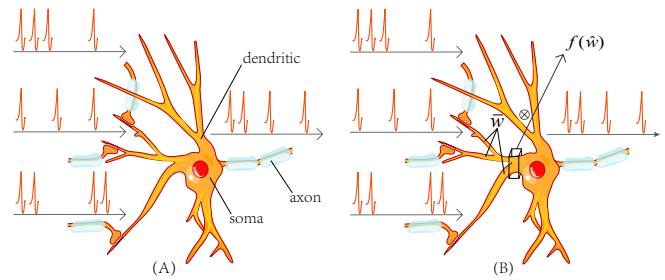


Figure 2: The illustration of the spiking neuron model and APBS learning mechanism. (A) The dynamics of spiking neurons. Neurons accumulate weighted spikes to membrane potential and generate spikes once the membrane potential exceeds a threshold. (B) The details of the APBS learning mechanism, which extracts shared weights from original weights.

The second is to train SNNs directly. For example, [Lagorce *et al.*, 2017] and [Sironi *et al.*, 2018] use (averaged) time surfaces structures to process the temporal information of SNNs. Based on spike-timing-dependent plasticity (STDP) rule [Bi and Poo, 1998], [Zhang *et al.*, 2018] uses brain-inspired principles to train SNNs. Furthermore, the method of finding an approximate gradient for non-differentiable spikes has become very popular in recent years. Among these methods, [Zheng *et al.*, 2021] performs back-propagation (STBP) along with the spatial and temporal domains of SNNs. In contrast, [Wu *et al.*, 2021] uses the accumulated spikes as an alternative gradient to avoid the huge memory consumption brought by the STBP method. Our method falls into this category.

2.2 Neuromorphic Data augmentation

Data augmentation is an explicit form of regularization that is also widely used in the training of ANNs. The two most popular and effective data augmentation methods in ANNs are random cropping [Krizhevsky *et al.*, 2012] and random flipping [Simonyan and Zisserman, 2015]. Random flipping randomly flips the input image horizontally, while random cropping extracts a random sub-patch from the input image. To the best of our knowledge, augmentation methods for neuromorphic data remain a blank slate to be explored.

3 Method

This section first briefly introduces the spiking neuron model and then analyzes the modeling approach of APBS. Methods for neuromorphic data augmentation are subsequently introduced. Finally, the training process of the network is shown.

3.1 Spiking Neuron Model

The dynamics of a biological neuron are shown in Figure 2 (A). The neuron membrane potential increases with the accumulation of weighted spikes, and an output spike is generated once the membrane potential exceeds a threshold. The widely used leaky integrate and fire model describes the

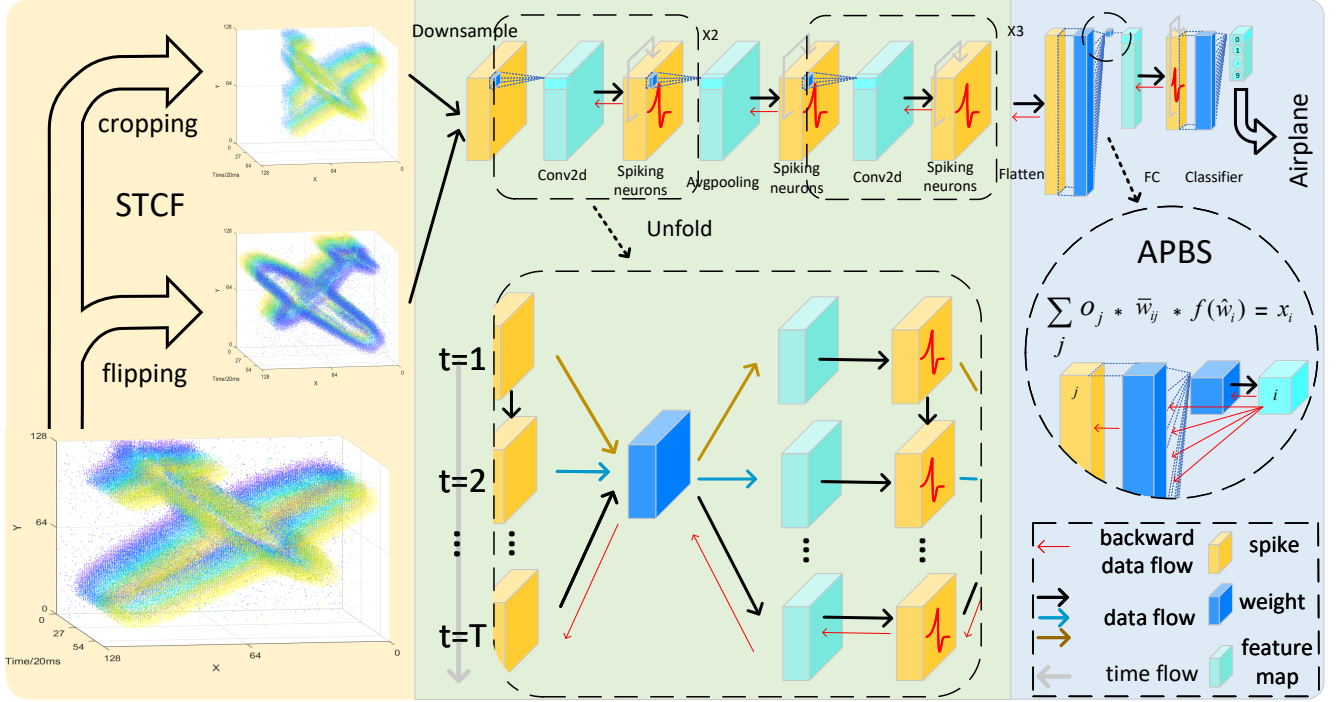


Figure 3: The architecture of our network. The left side represents the process of the proposed STCF method, the middle part shows the flow of the spiking neurons in the spatiotemporal domain, and the right part illustrates our proposed APBS method.

dynamics of the membrane potential as:

$$\left. \begin{aligned} \tau_m \frac{du}{dt} &= -(u - V_{rest}) + R_m \cdot I(t), & u < V_{th} \\ u &= V_{rest} \end{aligned} \right\}, & u \geq V_{th} \quad (1)$$

$$o = \delta(t - t_i)$$

where $\tau_m = R_m C_m$ is the membrane time constant, R_m and C_m are resistance constant and capacitance constant, respectively. u is the membrane potential, $I(t)$ is the input current, V_{th} and V_{rest} are the spiking threshold and resting potential. Once u reaches V_{th} at t_i , a spike is generated and u is reset to V_{rest} , which is usually taken as 0. The output spike o is described by the Dirac delta function $\delta(x)$. The input will be summed to $I(t)$ by the dendrite response weight w . To facilitate the calculation and simulation, Equation (1) is converted into a discrete form by Euler method. Given that the time interval dt is constant during simulation, $1 - dt/\tau_m$ and $1/C_m$ are absorbed into response weights w and leakage coefficient λ respectively. The discrete form of Equation (1) can be described as:

$$\begin{aligned} u_i^{n+1,t+1} &= \lambda u_i^{n+1,t} (1 - o_i^{n+1,t}) + x_i^{n+1,t+1} \\ x_i^{n+1,t+1} &= \sum_j w_{ij}^{n+1} o_j^{n,t+1} \\ o_i^{n+1,t+1} &= H(u_i^{n+1,t+1} - V_{th}) \end{aligned} \quad (2)$$

where n denotes the n -th layer and w_{ij} is the synaptic weight from the j -th neuron in pre-layer n to the i -th neuron in the post-layer $n + 1$. x_i denotes the weighted input and $H(x)$ is the Heaviside step function.

3.2 Associative Plasticity between Synapses

Motivation. The associative long-term potentiation phenomenon in Figure 1 illustrates that repeated stimulation of one synaptic afferent of a neuron can enhance the synaptic potential induced by another afferent stimulus of the same cell [DAVISON, 1985]. In short, there is an associative enhancement effect between synapses when stimulated concurrently. On the other hand, the associated long-term depressive phenomenon [Stanton and Sejnowski, 1989] corresponding to the ALTP phenomenon is also observed in hippocampal slices. Both of these phenomena indicate that there is associative plasticity between synapses.

Modeling. We model the associative plasticity between synapses inspired by the shape and connection of neurons. As shown in Figure 2 (B), the original weight is divided into two parts in series, one is the independent neuron coefficient \bar{w} corresponding to the dendritic terminal, and another is the extracted shared weight \hat{w} corresponding to the dendritic trunk. In this way, the \bar{w} emphasizes the effect of learning between neurons and \hat{w} emphasizes mutual influence between synapses. The original weight w_{ij}^{n+1} is formulated by:

$$w_{ij}^{n+1} = f(\hat{w}_i^{n+1}) \times \bar{w}_{ij}^{n+1} \quad (3)$$

$$d\bar{w}_{ij}^{n+1} = dw_{ij}^{n+1} \quad (4)$$

$$df(\hat{w}_i^{n+1}) = \sum_j \left(\frac{dw_{ij}^{n+1}}{\bar{w}_{ij}^{n+1}} \right) \quad (5)$$

where f is a function describing the change curve of the shared weight \hat{w} . $d\bar{w}_{ij}^{n+1}$ and dw_{ij}^{n+1} are the gradients of

\bar{w}_{ij}^{n+1} and w_{ij}^{n+1} respectively. Above formulae fit well with the phenomenon in Figure 1 for three reasons:

- Equation (3) indicates the neuron coefficient \bar{w} and shared weight \hat{w} jointly determine the input weights. While in Figure 1 (B), influences from other neurons and other synapses corporately determine the response to input stimuli.
- Equation (4) suggests that gradients do not change when propagating back along the shared weight. Corresponding to Figure 1 (A), influences between synapses can not change the backward information.
- Equation (5) denotes that the shared weight is determined by the sum of neuron weights. As shown in Figure 1 (A), interactions between synapses are induced by stimulation from other neurons.

Furthermore, since the biochemical mechanism of APBS is still unclear, we refine several update curves of the shared weights \hat{w} to explore the efficient form of function f . The simplest is $f(\hat{w}) = \hat{w}$, a monotonically increasing linear function. Besides, considering that the shared weight should be positive as a strengthening or debilitating factor, the absolute value function $f(\hat{w}) = abs(\hat{w})$ is adopted. Last but not least, the well-known ReLU function $f(\hat{w}) = relu(\hat{w})$ is introduced because the non-monotonic absolute value function may make learning turbulent. Experiments in Section 4 show the high performance of these curves.

3.3 Spatiotemporal Cropping and Flipping

Neuromorphic data are captured by event-based cameras, which only record dynamic events in the field of view, leading to severe overfitting while reducing the amount of information. Generally, each sample is represented by a number of events, which are described as:

$$e_i = [t_i, x_i, y_i, p_i], \quad i \in \{1, 2, \dots, I\} \quad (6)$$

where t_i is the timestamp at which the event is generated, x_i and y_i are the position of the pixel grid. p_i is the polarity of the event, a binary value meaning respectively OFF and ON events, and I is the number of events.

Inspired by the idea of crop and flip [Krizhevsky *et al.*, 2012; Simonyan and Zisserman, 2015], we propose a spatiotemporal cropping and flipping (STCF) method for event data, which can be formulated as:

$$d_i = c \cdot (D_B - D_A) + (-1)^c (d_i - D_A) \quad (7)$$

where d_i represents a generic expression for x_i , y_i , and t_i while $[D_A, D_B]$ is the corresponding cropping range randomly generated. $c \in \{0, 1\}$ indicates the random flipping parameter, set as 1 when flipping. The cropping area is first moved to the origin through $d_i - D_A$, and then flipped according to the parameter c . As shown on the left of Figure 3, the STCF method enhance the generalization of the network in the time domain.

3.4 Training Details

The forward process. The architectures we utilized are similar to other spiking convolutional neural networks [Lee

et al., 2020; Wu *et al.*, 2021; Wu *et al.*, 2019]. As illustrated in Figure 3, event data is cropped and flipped by Equation (7), and then downsampled to input spikes, which are weighted chronologically accumulated to the membrane potential of spiking neurons. The dynamics of the neuron are described by Equation (2). The output spikes are also fed into the next layer in chronological order, and the cycle repeats. The expanded section in the middle of Figure 3 illustrates the direction in which data travels through space and time. Since the gradients are only passed at the end, it does not keep the computation graph every step like space-temporal backpropagation. We measure the mean square error between the results and label vector \mathbf{Y} within a given time window T , which follows the setting in [Lee *et al.*, 2020; Wu *et al.*, 2021]. The loss function is defined as:

$$L = \frac{1}{2} \left\| \mathbf{Y} - \frac{\mathbf{u}^{N,T}}{T \cdot V_{th}} \right\|_2^2 \quad (8)$$

where the V_{th} is the threshold and $\mathbf{u}^{N,T}$ denotes the membrane potential vector of the output layer in Equation (2).

The backward process: For the backpropagation method, the main target is to measure the gradient of each synaptic weight without omission accurately. We adopt the method of accumulating spiking flow [Wu *et al.*, 2021] as the baseline and supplement the mutual influence between synapses with the proposed APBS method. Therefore we use the accumulated output-input spikes ratio as a gradient. The ratio S_i^n can be formulated by [Wu *et al.*, 2021]:

$$S_i^n = \frac{\mathcal{FO}_i^n}{\mathcal{FT}_i^n} = \frac{\sum_{t=1}^T o_i^{n,t}}{\sum_{t=1}^T \sum_j w_{ij}^n o_j^{n-1,t}} \quad (9)$$

and the weight of the network can be updated by the following formula [Wu *et al.*, 2021]:

$$\frac{\partial L}{\partial w_{ij}^n} = \frac{\partial L}{\partial \mathcal{FO}_i^n} \frac{\partial \mathcal{FO}_i^n}{\partial \mathcal{FT}_i^n} \frac{\partial \mathcal{FT}_i^n}{\partial w_{ij}^n} = \frac{\partial L}{\partial \mathcal{FO}_i^n} S_i^n \mathcal{FO}_j^{n-1} \quad (10)$$

using the chain rule and the gradients of $f(\hat{w}_i^n)$ and \bar{w}_{ij}^n are formulated as:

$$\begin{aligned} \frac{\partial L}{\partial \bar{w}_{ij}^n} &= \frac{\partial L}{\partial w_{ij}^n} = \frac{\partial L}{\partial \mathcal{FO}_i^n} S_i^n \mathcal{FO}_j^{n-1} \\ \frac{\partial L}{\partial f(\hat{w}_i^n)} &= \sum_j \frac{\partial L}{\partial w_{ij}^n} \frac{\partial w_{ij}^n}{\partial f(\hat{w}_i^n)} = \sum_j \frac{\partial L}{\partial \mathcal{FO}_i^n} S_i^n \mathcal{FO}_j^{n-1} \bar{w}_{ij}^n \end{aligned} \quad (11)$$

It is worth mentioning that when the network is deployed on the chip, we can directly combine $f(\hat{w}_i^n)$ and \bar{w}_{ij}^n into w_{ij} . Thus the APBS learning mechanism will not add any operation in inference. In addition, signals in the network are transmitted in the form of spikes, including the input and pooling layers. Thus all the multiplications of the network can be replaced by logical AND $\&$, resulting in SNNs consuming orders of magnitude less energy than ANNs [Roy *et al.*, 2019]. Besides, it should be noted that in our model, biases are not introduced for calculation.

4 Experiments

In this section, we conduct extensive experiments to demonstrate the superior performance of the proposed methods. For

Datasets	Work	Method	Reference	Architecture	Acc.(%)
CIFAR10	[Wu <i>et al.</i> , 2019]	STBP	AAAI 2019	CIFARNet	90.53
	[Rathi <i>et al.</i> , 2020]	Hybrid	ICLR 2020	VGG-9	90.54
	[Zhang and Li, 2020]	TSSL-BP	NeurIPS 2020	CIFARNet	91.41
	[Wu <i>et al.</i> , 2021]*	ASF-BP	AAAI 2021	VGG-7	91.47
	Ours	APBS-STCF	–	VGG-7	91.81
MNIST-DVS	[Lagorce <i>et al.</i> , 2017]	Hots	TPAMI 2017	FE-FE-FE-SVM	80.3
	[Liu <i>et al.</i> , 2020]	SPA	AAAI 2020	HMAX	96.7
	[Sironi <i>et al.</i> , 2018]	Hats	CVPR 2018	FE-FE-FE-SVM	98.4
	[Ramesh <i>et al.</i> , 2020]	DART	TPAMI 2020	Bag-of-words	98.5
	Ours	APBS-STCF	–	VGG-7	99.6
CIFAR10-DVS	[Lagorce <i>et al.</i> , 2017]	Hots	TPAMI 2017	FE-FE-FE-SVM	27.1
	[Liu <i>et al.</i> , 2020]	SPA	AAAI 2020	HMAX	32.2
	[Sironi <i>et al.</i> , 2018]	Hats	CVPR 2018	FE-FE-FE-SVM	52.4
	[Bi <i>et al.</i> , 2019]	GCN	ICCV 2019	Conv-3* <i>Res_g</i> -2*FC	54.0
	[Wu <i>et al.</i> , 2019]	STBP	AAAI 2019	CIFARNet	60.5
	[Ramesh <i>et al.</i> , 2020]	DART	TPAMI 2020	Bag-of-words	65.8
	[Zheng <i>et al.</i> , 2021]	STBP-tdBN	AAAI 2021	ResNet-19	67.8
	[Wu <i>et al.</i> , 2021]*	ASF-BP	AAAI 2021	VGG-7	62.5
Ours	APBS-STCF	–	VGG-7	76.1	

Table 1: Performance comparison of the proposed method and the state-of-the-art methods on CIFAR10-DVS, MNIST-DVS and CIFAR10 datasets. The * symbol means that this is the baseline we reproduced. FE is short for feature extraction layer and *Res_g* is the graph resnet block. And the best results are in bold for clarity.

a fair comparison, we use the same hyperparameters and experimental settings with [Wu *et al.*, 2021], which is our baseline. Specifically, the weights of the convolutional and fully connected layers are initialized by a normal distribution. The threshold and leakage coefficients of neurons are belonged [0.9, 2]. Adam optimizer is introduced to adjust the learning rate which is initially set to 5×10^{-4} . Moreover, we apply the APBS learning mechanism on just one layer of neurons, as shown in Figure 3.

4.1 Datasets

We evaluate the performance of our methods on both neuromorphic datasets (MNIST-DVS, CIFAR10-DVS) and static datasets (CIFAR10).

MNIST-DVS datasets [Serrano-Gotarredona and Linares-Barranco, 2013]. It contains three scales (4, 8, 16) of the digits, each having 10,000 samples. The recordings contain noise, blur, and other factors caused by a fixed DVS camera when capturing the moving original digit images. We use scale 16 of the datasets and perform training with 90% of randomly chosen samples while testing with the remaining 1,000 samples. Time steps and batch size are 30 and 40, respectively.

CIFAR10-DVS datasets [Li *et al.*, 2017]. It consists of 10,000 samples from CIFAR10, taken by DVS camera like MNIST-DVS. It is a challenging recognition task due to the complexity of the samples. We follow previous works [Wu *et al.*, 2021; Zheng *et al.*, 2021] by randomly selecting 90% of the images as the training images and the rest images are testing images for every class. Furthermore, we downsample input images to the resolution of 42×42 as in previous work [Wu *et al.*, 2021]. Time steps and batch size are 100

and 40, respectively.

CIFAR10 datasets. It is very famous and widely used in deep learning for object classification. It contains 60,000 color images in 10 classes, of which 50,000 images are for training, and 10,000 images are for testing. We utilize a standard data augmentation strategy consisting of the random crop, random horizontal flip, random erase, and normalization. Poisson sampling is also applied for input. Time steps and batch size are 100 and 50, respectively.

4.2 Comparison with the State-of-the-Art

As shown in Table 1, we achieve the state-of-the-art performance on neuromorphic datasets and superior performance on static datasets. On the MNIST-DVS datasets, our model gets the classification accuracy of **99.6%** or 0.4% error rate. It should be pointed out that although [Sironi *et al.*, 2018] only uses a four-layer structure, it needs to calculate averaged time surface, which consumes more computing power. On the CIFAR10-DVS datasets, it can be seen that our model achieves **76.1%** accuracy, which outperforms other methods by a large margin. It is necessary to point out that the baseline only achieves 62.5% accuracy, and our methods deliver a 13.6% improvement. The bionic APBS method is also applicable to static datasets. On the CIFAR10 datasets, we achieve an accuracy of **91.81%**, which is also higher than other works with similar architecture sizes. Experimental results demonstrate that our methods are effective regardless of neuromorphic or static datasets.

4.3 Ablation Studies

We perform ablation experiments on different datasets to evaluate the effectiveness of each proposed component.

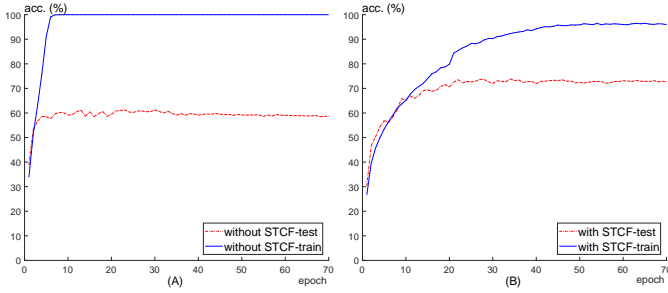


Figure 4: The performance of the training set and test set on CIFAR10-DVS datasets. (A) The learning curve without STCF method. (B) The learning curve with STCF method.

Methods	MNIST-DVS(%)	CIFAR10-DVS(%)
baseline	99.2	62.5
base+APBS	99.5	63.9
base+STCF	99.5	73.8
ALL	99.6	76.1

Table 2: The effectiveness of proposed methods on MNIST-DVS datasets and CIFAR10-DVS datasets.

Overall Ablation Studies

On neuromorphic datasets, the previous work [Wu *et al.*, 2021] is replicated as our baseline, then the APBS learning method and STCF method are respectively added to it. As shown in Table 2, the APBS method is effective on different bases, and the STCF method achieves a noticeable effect since it is the first neuromorphic data augmentation method. It is worth noting that on the CIFAR10-DVS datasets, the combined effect of our methods is better than the sum of the individual effects.

Ablation Studies on STCF

Captured by fixed event-based cameras, neuromorphic data records the changing points in the field of view, allowing for better capture of critical information. While the amount of information plummeted, it is more accessible to overfitting. As shown in Figure 4 (A), our model with VGG-7 architecture quickly achieves a full score on the training set, but is unable to fit more test set data earlier. We naturally propose the STCF method, the first neuromorphic data augmentation method. Figure 4 (B) illustrates the effect of STCF method. As expected, the model learns more slowly on the training set while degrading less on the test set. Since the STCF method increases the diversity of the spatiotemporal data, the generalization performance of the network is significantly improved. Besides, we also note that the STCF method is orthogonal to most existing methods, thus providing a higher baseline.

Ablation Studies on APBS

As described in Section 3.2, different variation curves of shared weights are evaluated on CIFAR10-DVS datasets with the Resnet-9 network. The control variable method is used for a fair comparison, and all configurations are the same except the APBS method. The curves, including $f(\hat{w}) = \hat{w}$,

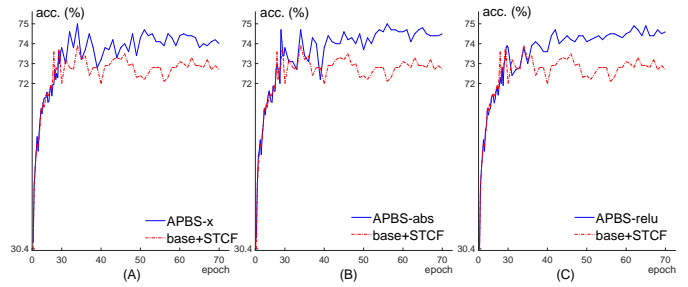


Figure 5: Performance with different functions of APBS method compared to experiments without APBS on CIFAR10-DVS datasets. (A) Performance with APBS-x method. (B) Performance with APBS-abs method. (C) Performance with APBS-relu method.

Methods	VGG-7(%)	Resnet-9(%)
baseline	62.5	61.3
base+STCF	73.8	73.9
base+STCF+APBS-x	74.8	75.0
base+STCF+APBS-abs	75.0	75.0
base+STCF+APBS-relu	76.1	74.9

Table 3: The effectiveness of APBS functions on CIFAR10-DVS datasets with different architectures.

$f(\hat{w}) = abs(\hat{w})$ and $f(\hat{w}) = relu(\hat{w})$, are marked as APBS-x, APBS-abs, APBS-relu, respectively. As shown in Figure 5, the blue lines represent APBS methods and the red lines show the control group without APBS methods. It turns out that the performances of these curves are comparable and significant, indicating that the APBS method is robust and effective.

Furthermore, multiple architectures are introduced to evaluate the robustness of the methods, including the most popular residual network structure. Table 3 shows that the APBS learning methods and STCF method are also effective and robust for different network structures.

5 Conclusion

In this work, we propose the associative plasticity between synapses (APBS) mechanism for SNNs. It is inspired by the associative long-term potential phenomenon observed in the mammalian brain. By making complementary modifications between synapses, APBS captures more learning signals and strengthens the ability of SNNs to fully explore spatiotemporal information. In addition, we propose a spatiotemporal cropping and flipping (STCF) method for neuromorphic data augmentation. The proposed methods achieve the state-of-the-art performance on the neuromorphic datasets, which indirectly indicates the biological plausibility of methods. Since the methods are orthogonal to existing methods, they provide a better baseline for future research. We are excited about the future of the APBS mechanism and STCF data augmentation method and plan to generalize them for other vision tasks. We believe that associative plasticity between synapses can enhance learning in SNNs, which will surely become a pillar for further exploration of brain-like computing.

References

- [Akopyan *et al.*, 2015] Filipp Akopyan, Jun Sawada, Andrew Cassidy, and et al. Truenorth: Design and tool flow of a 65 mw 1 million neuron programmable neurosynaptic chip. *IEEE Transactions on Computer-Aided Design of Integrated Circuits and Systems*, 34(10):1537–1557, 2015.
- [Barrionuevo and Brown, 1983] G Barrionuevo and T H Brown. Associative long-term potentiation in hippocampal slices. *Proceedings of the National Academy of Sciences*, 80(23):7347–7351, 1983.
- [Bi and Poo, 1998] Guo Qiang Bi and Mu Ming Poo. Synaptic modifications in cultured hippocampal neurons: Dependence on spike timing, synaptic strength, and postsynaptic cell type. *Journal of Neuroscience*, 18, 1998.
- [Bi *et al.*, 2019] Yin Bi, Aaron Chadha, Alhabib Abbas, and et al. Graph-based object classification for neuromorphic vision sensing. In *ICCV*, October 2019.
- [Cheng *et al.*, 2020] Xiang Cheng, Yunzhe Hao, Jiaming Xu, and Bo Xu. Linn: Improving spiking neural networks with lateral interactions for robust object recognition. In *IJCAI*, pages 1519–1525, 7 2020. Main track.
- [Davies *et al.*, 2018] Mike Davies, Narayan Srinivasa, Tsung Han Lin, and et al. Loihi: A neuromorphic manycore processor with on-chip learning. *IEEE Micro*, 38(1):82–99, 2018.
- [DAVISON, 1985] A. N. DAVISON. From neuron to brain. *Biochemical Society Transactions*, 13, 1985.
- [Ding *et al.*, 2021] Jianhao Ding, Zhaofei Yu, Yonghong Tian, and Tiejun Huang. Optimal ANN-SNN conversion for fast and accurate inference in deep spiking neural networks. In *IJCAI*, pages 2328–2336. ijcai.org, 2021.
- [Han *et al.*, 2020] Bing Han, Gopalakrishnan Srinivasan, and Kaushik Roy. Rmp-snn: Residual membrane potential neuron for enabling deeper high-accuracy and low-latency spiking neural network. In *CVPR*, June 2020.
- [Krizhevsky *et al.*, 2012] Alex Krizhevsky, Ilya Sutskever, and Geoffrey E Hinton. Imagenet classification with deep convolutional neural networks. In *NeurIPS*, volume 25, 2012.
- [Lagorce *et al.*, 2017] Xavier Lagorce, Garrick Orchard, Francesco Galluppi, and et al. Hots: A hierarchy of event-based time-surfaces for pattern recognition. *TPAMI*, 39(7):1346–1359, 2017.
- [Lecun *et al.*, 2015] Yann Lecun, Yoshua Bengio, and Geoffrey Hinton. Deep learning. *Nature*, 521, 2015.
- [Lee *et al.*, 2020] Chanky Lee, Syed Shakib Sarwar, Priyadarshini Panda, and et al. Enabling spike-based backpropagation for training deep neural network architectures. *Frontiers in Neuroscience*, 14:119, 2020.
- [Li *et al.*, 2016] Da Li, Xinbo Chen, Michela Becchi, and Ziliang Zong. Evaluating the energy efficiency of deep convolutional neural networks on cpus and gpus. In *BDCloud-SocialCom-SustainCom*, pages 477–484, 2016.
- [Li *et al.*, 2017] Hongmin Li, Hanchao Liu, Xiangyang Ji, and et al. Cifar10-dvs: An event-stream dataset for object classification. *Frontiers in Neuroscience*, 11:309, 2017.
- [Liu *et al.*, 2020] Qianhui Liu, Haibo Ruan, Dong Xing, and et al. Effective aer object classification using segmented probability-maximization learning in spiking neural networks. *AAAI*, 34(02):1308–1315, Apr. 2020.
- [Maass, 1997] Wolfgang Maass. Networks of spiking neurons: The third generation of neural network models. *Neural Networks*, 10(9):1659–1671, 1997.
- [Ramesh *et al.*, 2020] Bharath Ramesh, Hong Yang, Garrick Orchard, and et al. Dart: Distribution aware retinal transform for event-based cameras. *TPAMI*, 42(11):2767–2780, 2020.
- [Rathi *et al.*, 2020] Nitin Rathi, Gopalakrishnan Srinivasan, Priyadarshini Panda, and Kaushik Roy. Enabling deep spiking neural networks with hybrid conversion and spike timing dependent backpropagation. In *ICLR*, 2020.
- [Roy *et al.*, 2019] Kaushik Roy, Akhilesh Jaiswal, and Priyadarshini Panda. Towards spike-based machine intelligence with neuromorphic computing. *Nature*, 575, 2019.
- [Serrano-Gotarredona and Linares-Barranco, 2013] Teresa Serrano-Gotarredona and Bernabé Linares-Barranco. A 128×128 1.5% contrast sensitivity 0.9% FPN 3 μ s latency 4 mw asynchronous frame-free dynamic vision sensor using transimpedance preamplifiers. *IEEE Journal of Solid-State Circuits*, 48(3):827–838, 2013.
- [Simonyan and Zisserman, 2015] Karen Simonyan and Andrew Zisserman. Very deep convolutional networks for large-scale image recognition. *ICLR*, 2015.
- [Sironi *et al.*, 2018] Amos Sironi, Manuele Brambilla, Nicolas Bourdis, Xavier Lagorce, and Ryad Benosman. Hats: Histograms of averaged time surfaces for robust event-based object classification. In *CVPR*, June 2018.
- [Stanton and Sejnowski, 1989] Patric K. Stanton and Terrence J. Sejnowski. Associative long-term depression in the hippocampus induced by hebbian covariance. *Nature*, 339, 1989.
- [Wu *et al.*, 2019] Yujie Wu, Lei Deng, Guoqi Li, and et al. Direct training for spiking neural networks: Faster, larger, better. *AAAI*, 33(01):1311–1318, Jul. 2019.
- [Wu *et al.*, 2021] Hao Wu, Yueyi Zhang, Wenming Weng, and et al. Training spiking neural networks with accumulated spiking flow. *AAAI*, 35(12):10320–10328, May 2021.
- [Zhang and Li, 2020] Wenrui Zhang and Peng Li. Temporal spike sequence learning via backpropagation for deep spiking neural networks. *NeurIPS*, 2020-December, 2020.
- [Zhang *et al.*, 2018] Tielin Zhang, Yi Zeng, Dongcheng Zhao, and Bo Xu. Brain-inspired balanced tuning for spiking neural networks. In *IJCAI*, pages 1653–1659, 7 2018.
- [Zheng *et al.*, 2021] Hanle Zheng, Yujie Wu, Lei Deng, Yifan Hu, and Guoqi Li. Going deeper with directly-trained larger spiking neural networks. *AAAI*, 35(12):11062–11070, May 2021.